A theoretical examination of localized nanoscale induction by single domain magnetic particles

(iD) **Michael G. Christiansen,** (iD) **Nima Mirkhani,** (iD) **William Hornslien, et al.**

ARTICLES YOU MAY BE INTERESTED IN

A theoretical examination of localized nanoscale induction by single domain magnetic particles

Michael G. Christiansen,[1,a)] (iD) Nima Mirkhani,[1] (iD) William Hornslien,[2] (iD) and Simone Schuerle[1,b)] (iD)

AFFILIATIONS

[1]Department of Health Sciences and Technology, ETH Zurich, 8093 Zurich, Switzerland
[2]Department of Mathematical Sciences, Norwegian University of Science and Technology, 7034 Trondheim, Norway

[a)]Author to whom correspondence should be addressed: michael.christiansen@hest.ethz.ch
[b)]Electronic mail: simone.schuerle@hest.ethz.ch

ABSTRACT

Single domain magnetic nanoparticles are increasingly investigated as actuators of biological and chemical processes that respond to externally applied magnetic fields. Although their localized effects have often been attributed to nanoscale heating, recent experimental evidence suggests the need to consider alternative hypotheses. Here, using the stochastic Landau–Lifshitz–Gilbert equation and finite element modeling, we investigate and critically examine an alternative hypothesis that localized effects may instead involve the induced electric fields arising from the dynamical behavior of individual single domain magnetic particles. We model the magnetization dynamics and resulting induced electric fields for two relevant and distinct cases of magnetic nanoparticles in alternating magnetic fields: (1) magnetogenetic stimulation of channel proteins associated with ferritin and (2) catalytic enhancement of electrochemical hydrolysis. For the first case, while the local electric fields that ferritin generates are shown to be insufficient to perturb the transmembrane potential, fields on the surface of its mineral core on the order of 10^2–10^3 V/m may play a more plausible role in mass transport of iron ions that indirectly lead to stimulation. For the second case, our model indicates that the highest interfacial electric field strengths, on the order of 10^2 V/m, are expected during reversal events. Thus, nanoparticles well suited for hysteresis heating can also act as intermittent sources of localized induced electric fields in response to an alternating applied field. Finally, we compare the magnitude and timescale of these electric fields to technologically relevant phenomena, showing that they are generally weaker and faster.

I. INTRODUCTION

Single domain magnetic nanoparticles (MNPs) are increasingly investigated as nanoscale actuators that enable wireless control or enhancement of biological and chemical processes in a variety of applied contexts. Commonly, these effects have been attributed to hysteretic heat dissipation, with quasimagnetostatic alternating magnetic fields (AMFs) in the kilohertz or megahertz frequency range serving to couple these nanoparticles to an external circuit. The abundance of biomedical applications employing this concept reflects the underlying appeal of wireless actuation as a basis for minimally invasive manipulation. For example, MNPs exposed to AMFs have been demonstrated to modulate the anticancer activity of nanozymes,[1,2] trigger release of liposomal cargo,[3–5] and to influence the composition of the protein corona formed in vivo.[6] More controversially, a broad set of techniques known as magnetogenetics

has sought to genetically impart magnetic control over cellular activity, usually by expressing the Fe storage protein ferritin in association with heat sensitive ion channels.[7,8] Apart from medicine, the use of nanoscale effects of MNPs in AMFs has been suggested for purposes such as regulating catalytic activity of enzymes[9] or enhancing the electrochemical production of hydrogen.[10]

As the application space of MNPs widens, intriguing questions can be raised regarding the exact nature of the phenomena that underpin their nanoscale actuation effects. Typically, these effects have been attributed to a temperature increase within a few nanometers of their surfaces. Whereas the heating of a millimeter scale droplet of a concentrated suspension of MNPs is anticipated by bulk heat transport, a nanoscale temperature increase is not anticipated in aqueous solutions around isolated MNPs.[11] As an analogous nonmagnetic system, plasmonic gold nanoparticles comparable in size to

MNPs irradiated by lasers have been found to elevate their surface temperatures, yet they dissipate substantially more heat per particle and this behavior is in reasonable agreement with bulk heat transport.[12,13] Empirically probing temperature around MNPs with nanoscale resolution requires indirect readouts, and experiments have been performed in which the breaking of chemical bonds,[14] changes in dye fluorescence,[15] or similar signals have been interpreted as indicating nanoscale temperature gradients. Similar types of experiments with careful controls have recently produced unexpected null results,[16,17] suggesting that the nanoscale phenomena underpinning actuation may be more nuanced than originally thought and relate somehow to their magnetic properties. One perceptive suggestion has been that the intermittent nature of heat release during magnetic hysteresis may lead to transient heat spikes with greater instantaneous power.[17] Alternatively, by focusing on the details of magnetization reversal in individual particles, it is also possible to consider physical processes other than heating to attempt to explain nanoscale actuation mediated by MNPs.

Here, we critically examine the possibility that localized induced electric fields may play some role in explaining effects previously attributed to nanoscale heating. The possible relevance of detailed magnetization dynamics of superparamagnetic moments to nanoscale effects has been previously suggested[18] but does not appear to have yet been seriously considered. This is perhaps due to the small scale of MNPs or because modeling hysteresis typically averages reversal behavior over large ensembles of MNPs and over long timescales relative to the GHz fluctuations of their magnetic moments. For most applications, the detailed dynamical behavior of individual magnetic moments can be safely neglected. Nevertheless, the magnetization of individual MNPs has long been understood to rapidly precess during coherent reversal and thermal fluctuation,[19] a phenomenon that can be expected to dominate the locally induced electric fields. Using the stochastic Landau–Lifshitz–Gilbert equation (sLLG) to predict the dynamical behavior

of MNPs, we examine localized induced electric fields, focusing on two important cases (Fig. 1).
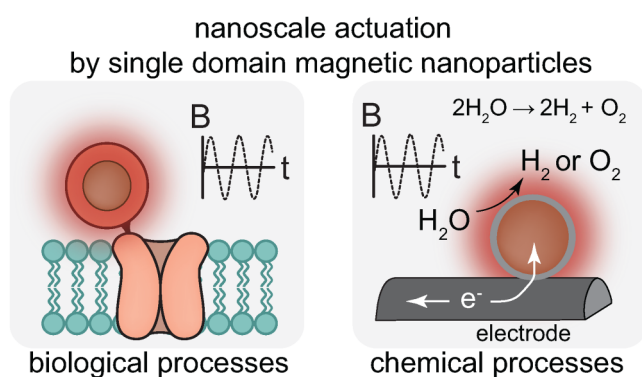
In the first case, we examine possible roles for induced electric fields in ferritin-based magnetogenetics, a set of techniques in which transgenic ion channels incorporating ferritin have reportedly enabled magnetic control over neuronal activity. Magnetogenetics and its proposed mechanisms remain a source of controversy because it has been difficult to replicate experimentally and the exceedingly weak magnetic moment of ferritin seems to preclude the possibility of direct actuation.[20] Despite its weak magnetic moment of about $300\,\mu_B$,[21–23] the work presented here predicts that ferritin produces surprisingly high electric field magnitudes in its immediate vicinity relative to a comparatively larger magnetite particle. Nevertheless, our analysis ultimately finds that these electric fields are too weak to allow sufficient interaction with the gating charges of ion channel proteins to influence their function. Even so, electric fields at the surface of ferritin's mineral core may still offer a mechanistic clue linking Fe ion release and applied magnetic fields in magnetogenetics.

In the second case, we consider the magnitude of electric fields occurring at the surface of metallic iron carbide nanoparticles that have been reported to enhance electrochemical production of hydrogen through nanoscale heating effects.[10] The magnetic properties and dynamic behavior of these catalytic MNPs differ markedly from ferritin, exhibiting far higher magnetization and tending to trap the magnetic moments close to the easy axes between comparatively rarer reversal events. Because the scale of the induced electric fields depends on the angle of precession, we find that the electric field magnitude increases significantly during reversal events that are correlated with hysteresis heating.

In both case studies, the induced electric fields are surprisingly large, yet far smaller than the electric fields inherently present in the neuronal membrane or in accumulations of interfacial charge at an electrode. The rapidity of magnetic precession accounts for these unexpectedly large electric field values, yet simultaneously explains why these fields vary too quickly for capacitive effects to further magnify interfacial electric fields. We conclude by discussing possibilities for experimental investigation and the considering implications of our findings on the design of MNPs as nanoscale actuators intended to exploit these effects.

II. MODELING ELECTRIC FIELDS GENERATED FROM DYNAMICAL BEHAVIOR OF SUPERPARAMAGNETIC MOMENTS

To simulate the dynamical behavior of single domain MNPs with properties corresponding to the cases of interest, we numerically solved the sLLG equation using scripts implemented primarily in Python. Because the basic physics of the sLLG equation is well established and its numerical solution is well-studied in the existing literature,[25] a conceptual overview of our model is provided here with emphasis on validation for the relevant application cases. Additional details, as well as representative Python scripts can be found in supplementary material, Secs. S1 and S2, respectively. The sLLG equation describes precession of the magnetic moment of

**nanoscale actuation
by single domain magnetic nanoparticles**

biological processes

chemical processes

$2H_2O \rightarrow 2H_2 + O_2$

FIG. 1. Single domain magnetic nanoparticles have increasingly been used as nanoscale actuators, coupling externally applied magnetic fields to biological processes such as the opening of channel proteins (left) or chemical processes such as catalysis (right). Although these effects are frequently attributed to nanoscale heating, the actual mechanism remains unclear.

single domain MNPs under thermal agitation,[19,26,27]

$$\frac{d\boldsymbol{\alpha}}{dt} = -\gamma_1\,\boldsymbol{\alpha}\times\mathbf{H_{eff}} - \kappa\gamma_1\,\boldsymbol{\alpha}\times(\boldsymbol{\alpha}\times\mathbf{H_{eff}}).\quad(1)$$

Here, $\boldsymbol{\alpha}$ is a unit vector corresponding to the magnetization direction of the particle, t is the time, and κ is a unitless damping constant. γ_1 is related to κ, the permeability of free space μ_0, and the gyromagnetic ratio γ as follows:

$$\gamma_1 = \frac{\mu_0\gamma}{1+\kappa^2}.\quad(2)$$

The effective field $\mathbf{H_{eff}}$ is defined in terms of the overall energy function U of the moment m of a particle,

$$\mathbf{H_{eff}} = -\frac{1}{\mu_0 m}\frac{\partial U}{\partial\boldsymbol{\alpha}}.\quad(3)$$

$\mathbf{H_{eff}}$ can be broken into a sum of several contributions,

$$\mathbf{H_{eff}} = \mathbf{H_{ap}} + \mathbf{H_k} + \mathbf{H_{th}}.\quad(4)$$

Here, $\mathbf{H_{ap}}$ is the applied field, $\mathbf{H_k}$ is a term that captures the influence of anisotropy, and $\mathbf{H_{th}}$ is the thermal field, a stochastic term. For uniaxial anisotropy, $\mathbf{H_k}$ can be expressed in terms of the barrier energy U_B separating the easy axes,

$$\mathbf{H_k} = \frac{2U_B}{\mu_0 m}\begin{pmatrix}\alpha_x\\\alpha_y\\0\end{pmatrix}.\quad(5)$$

$\mathbf{H_{th}}$ is defined according to statistical properties,

$$H_{th,i}(t)H_{th,j}(t') = \phi\delta_{i,j}\delta(t-t'),\quad(6)$$

where ϕ is a constant proportional to $k_B T$ and inversely proportional to m.[19] Except where explicitly stated otherwise, a temperature of 300 K was assumed for all simulations shown in this work. To solve Eq. (1), we employed a fourth order Runge–Kutta algorithm to advance the system in time, renormalizing the unit vector $\boldsymbol{\alpha}$ after each timestep. For the *ith* component of $\mathbf{H_{th}}$, stochastic noise was introduced by a multiplying constant H_{th0} with a normally distributed random variate. Since the magnitude of H_{th0} depends on both physical parameters and features of the model such as the timestep, its value was determined empirically by removing anisotropy and iteratively fitting H_{th0} to produce the magnetization expected at a single point of the expected Langevin function. The result of propagating the system forward in time is precession of the magnetic moment of the single domain MNPs, subject to thermal fluctuation [Fig. 2(a)]. Time evolution of the z projection of $\boldsymbol{\alpha}$ [Fig. 2(b)] shows that the magnetic moment tends to be oriented along one of its preferred axes with occasional stochastic jumps between preferred directions, a behavior that has also been observed experimentally at lower temperatures and longer timescales.[28]

As a first step in validating the model, we assessed its convergence to the Langevin function, an analytical expression for the equilibrium behavior expected for ensembles of freely orienting magnetic moments in an applied field. By removing the contribution of anisotropy to the effective field, maintaining a consistent value for H_{th0}, and calculating time-averaged magnetization vs applied field, good convergence to the Langevin function is found for the MNPs modeled in this study [Fig. 2(c)].

Basic descriptions of dynamical behavior of anisotropic magnetic nanoparticles typically emphasize the Néel–Arrhenius relationship, which describes temperature dependence of stochastic reversal between preferred axes over an anisotropy energy barrier.[29] In the absence of an applied field, the timescale of stochastic reversal τ can be expressed as a function of an attempt rate τ_0, the magnitude of the intrinsic anisotropy barrier U_B, the Boltzmann constant k_B, and the absolute temperature T,

$$\tau = \tau_0\exp\left(\frac{U_B}{k_B T}\right).\quad(7)$$

Varying the temperature by rescaling the stochastic term in the sLLG equation and extracting distributions of lifetimes between reversal events, $\ln\tau$ vs $1/T$ can be plotted [Fig. 2(d)]. The linearity of these curves shows convergence to expected functional behavior, and fitting these curves reproduces the values for U_B that are assumed by the model. The order of magnitude of the attempt rates suggested from these fits agrees well with values extracted from characterization of reconstituted ferritin[21] and the values typically assumed in modeling magnetite particles.[30] Since these were not direct input parameters for the sLLG model, it suggests that the model is capturing physical features salient to predicting dynamic behavior.

Next, to model the induced electric field arising from the changing magnetic moment of nanoparticles, Maxwell's equations were numerically solved using the finite element method for magnetic moments representing single domain MNPs evolving in time,

$$\nabla\times\mathbf{H} = \mathbf{J} + \frac{\partial\mathbf{D}}{\partial t},\quad \nabla\times\mathbf{E} = -\frac{\partial\mathbf{B}}{\partial t},$$
$$\nabla\cdot\mathbf{B} = 0,\quad \nabla\cdot\mathbf{D} = \rho.\quad(8)$$

Here, $\mathbf{J}$ represents the current density, $\mathbf{D}$ is electric flux density, $\mathbf{E}$ is the electric field, and ρ is electric charge density. Along with the following constitutive relations, these form the set of partial differential equations that describe distribution of electric and magnetic fields in the vicinity of the nanoparticles:

$$\mathbf{D} = \epsilon_0\epsilon_r\mathbf{E},\quad(9)$$

$$\mathbf{B} = \mu_0\mu_r\mathbf{H},\quad(10)$$

$$\mathbf{J} = \sigma\mathbf{E}.\quad(11)$$

Here, ϵ_0 is the permittivity of vacuum, ϵ_r is the relative permittivity, μ_0 is the vacuum permeability, and μ_r is the relative permeability. σ is the electrical conductivity.
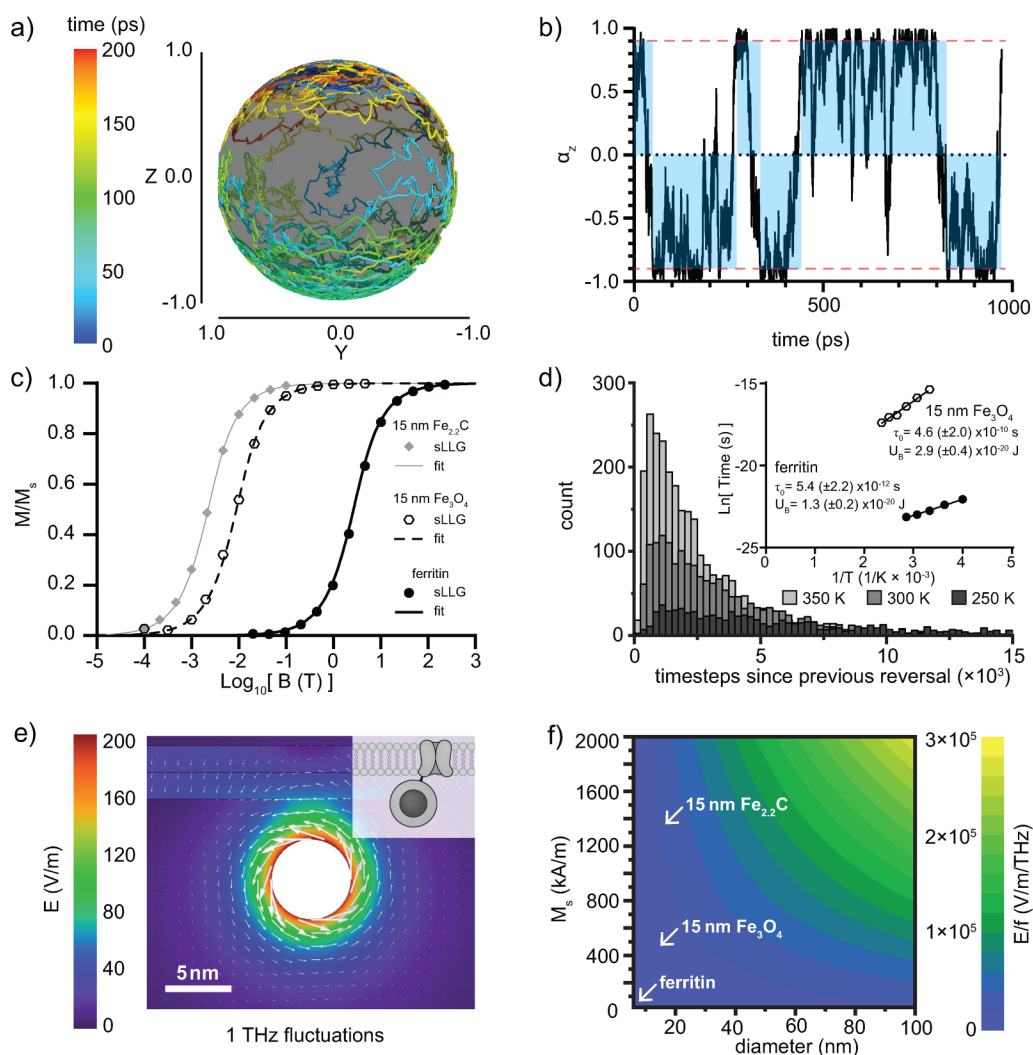
FIG. 2. Preliminary validation of the model for dynamical behavior of magnetic nanoparticles and resulting induced electric fields. (a) 200 ps of the time evolution of the orientation of the magnetic moment of ferritin in the absence of an applied field at a temperature of 300 K. Plot created with Mayavi in Python.[24] (b) Z projection of the unitless magnetization α of the magnetic moment of ferritin showing stochastic fluctuation over its energy barrier under the same conditions. The red dashed line indicates the threshold value $\alpha_z = \pm 0.9$ at which the moment is considered to have transited the easy axis. Blue shaded regions indicate periods between reversal events. (c) Langevin functions shown for particles at 300 K with anisotropy removed, possessing the same moments as ferritin (solid line), 15 nm magnetite particles (dashed line), and 15 nm $Fe_{2.2}C$ (gray line). Time-averaged magnetization predicted from the sLLG model vs applied field for ferritin (solid points), 15 nm magnetite (open hexagons), and 15 nm $Fe_{2.2}C$ (gray diamonds). Each point is the average of a simulation with 6×10^6 to 6×10^7 steps. (d) Histogram of timesteps elapsed since previous reversal over the barrier for the ferritin model at three temperatures investigated by rescaling the thermal field term (250, 300, and 350 K) in the absence of an applied field. Mean timescale of reversal over anisotropy barriers in the absence of an applied field was extracted, with results fitted in terms of the Néel–Arrhenius model for temperature dependence of relaxation rate on temperature (the inset). Fitted values are shown with uncertainty reflecting 95% confidence intervals in the linear fits. (e) Induced electric fields are plotted for a ferritin moment fluctuating at 1 THz near a membrane. (Assumed geometry detailed in the inset.) (f) A generalized parameter space considers the magnitude of the electric field induced at the surface of hypothetical single domain MNPs spanning a size range from 6 to 100 nm diameter and a magnetization from 20 to 2000 kA/m. Values for the MNPs modeled in this work have been mapped onto this parameter space, as indicated by the white labels. The electric field magnitude varies linearly with frequency, and the values shown are normalized to 1 THz fluctuations.

For the magnetogenetics case study described in Sec. III, a simplified 3D geometry of a nanoparticle located at the cytoplasmic side of the plasma membrane was reconstructed in COMSOL Multiphysics, where the Magnetic Fields interface was employed as the numerical solver. The computational domain consisted of four subdomains representing cytoplasm, nanoparticle, plasma membrane, and extracellular medium. Frequency-dependent conductivities and relative permittivities were assigned to each subdomain, as explained in greater detail in supplementary material, Sec. S3.

Under the predicted dynamical behavior of the magnetic moment of the nanoparticle, the set of coupled partial differential equations was solved for magnetic vector potential, from which the induced electric field was extracted using Faraday's law. In instances where harmonic oscillation of the magnetic moment at fixed frequencies was considered, analysis was conducted in the frequency domain. A 100-ps time-dependent study was carried out by using fluctuation of the magnetic moment predicted by the sLLG model as the input to assess the transmembrane voltage as a function of time. Because the induced electric field is non-conservative, different paths were defined normal to the membrane and adjacent to the nanoparticle to measure the induced voltage V_{ind} between two points p_1 and p_2 using the following path integral:

$$V_{ind} = -\int_{p_1}^{p_2} \frac{\partial \mathbf{A}}{\partial t} d\mathbf{r}, \tag{12}$$

where $\mathbf{A}$ represents the magnetic vector potential.

Before applying Maxwell's equations to the results of our sLLG model, an upper bound for the inductive effects of ferritin in the vicinity of a neuronal membrane was estimated by considering the electric fields produced by harmonic oscillation at a frequency of 1 THz [Fig. 2(f)]. Although assuming harmonic variation of the moment of ferritin is inherently artificial, Sec. III will show that the electric fields induced by ferritin include contributions from precession in the 100 s of GHz, as well as higher frequency contributions from stochastic variation. Thus, 1 THz was taken as the uppermost order of magnitude for relevant contributions. As a more general sweep of the relevant parameter space, induced electric fields were calculated at the surface of MNPs of varying size (6–100 nm), magnetization (20–2000 kA/m), and frequency (1 GHz–1 THz). Over the investigated frequency range, the peak electric field was found to scale linearly with the frequency, allowing the representation shown in Fig. 2(g), in which induced electric field strength is normalized to frequency.

III. A ROLE FOR NANOSCALE INDUCTION BY FERRITIN IN MAGNETOGENETICS?

A. Controversy over the mechanism of magnetogenetic stimulation

To exert targeted control over cellular activity in model organisms, biologists and neuroscientists have developed powerful techniques to introduce genes coding for channel proteins that, when expressed, sensitize neurons or other cell types to specific stimuli.[31,32] Initially, the preferred stimuli were visible light (optogenetics) or chemical substances (chemogenetics), however considerable interest later emerged in developing an analogous approach with magnetic fields for noninvasive actuation (magnetogenetics). Reports of conferred sensitivity to magnetic fields through fusion or targeting of one or more units of the Fe storage protein ferritin to a transient receptor potential vanniloid channel protein (TRPV1 or TRPV4) first appeared nearly a decade ago,[7,8] yet independent attempts to replicate these findings have often struggled to do so[33] and completely satisfactory mechanistic explanations have not been forthcoming. The presumptions that originally guided these efforts, namely, that mechanical or thermal cues might act directly on

TRPV channels to trigger Ca^{2+} influx, have been shown to be physically implausible[20] or to require a version of ferritin with highly unrealistic magnetic properties.[18] While synthetic magneto-ferritins can exhibit considerably larger magnetic moments, their synthesis requires markedly non-physiological conditions,[34] making them irrelevant to the cases studied here. Considering only ferritins produced biologically or under physiological conditions, their small magnetic moments ensure that their interaction with attainable magnetic fields is far too weak for mechanical actuation. Hysteresis heating of biologically produced ferritins is demonstrably negligible,[16] and even if extraordinary heat flow were to occur, its small size ensures that a local temperature increase is not expected.[20]

Although simple physical arguments compellingly rule out the direct magnetic interaction of ferritin with an external field as a mechanism for actuation, this reasoning leaves open the possibility of an indirect role for ferritin. We hypothesized that ferritin might act as a source of stochastic inductive perturbation coupled to voltage-sensitive channel proteins, sensitizing these channels to larger scale subthreshold inductive stimuli. Because the use of rapidly varying fields to stimulate unmodified neurons in transcranial magnetic stimulation (TMS) is extensively documented,[35] the role of ferritin expression in this scenario would not be to deliver the energy to reconfigure the channel proteins but rather to generate a perturbation that effectively lowers the kinetic barrier to activation. TMS typically employs pulses with peak amplitudes greater than 1 T and dB/dt values on the order of 10^4 T/s,[36] although stimulation thresholds are complex, depending also on pulse characteristics,[37] among other factors. Some of the reported instances of magnetogenetics involve quasimagnetostatic fields with comparatively lower amplitudes than TMS (tens of mT) that are pulsed or alternate at 100s of kHz, and their authors have suggested that time variation of the applied field may be a necessary aspect of the stimulus.[38]

Another indirect mechanism of actuation by ferritin has been recently suggested to involve the magnetically triggered release of Fe^{2+} and subsequent generation of reactive oxygen species.[39,40] Experimental evidence does appear to support this idea, showing that ferritin releases Fe content in the presence of MHz frequency fields at the timescale of seconds or minutes[41] and that reactive oxygen species are implicated in magnetogenetic stimulation.[39] While these studies may help clarify the role of ferritin in magnetogenetics, the mechanism is still not yet fully satisfying from a physical perspective because it does not explain how applied fields lead to Fe^{2+} release. Here too, it is worthwhile to consider whether nanoscale induction may contribute, especially since induced electric fields are expected to be strongest at the surface of ferritin's mineral core.

In this section, we analyze the localized inductive effects predicted by a realistic model of ferritin and consider its implications on the plausibility of these two potential indirect mechanisms of stimulation for excitatory cells. Despite the remarkably high rate of change of the magnetic flux density dB/dt predicted in its immediate vicinity, and its ability to induce electric fields comparable to a representative magnetite particle, ultimately we conclude that the resulting electric fields generated by ferritin are insufficient to perturb nearby voltage-gated ion channels. The influence of induced electric fields at the surface of the mineral core of ferritin

appears to be a more relevant physical factor for explaining magnetogenetic stimulation, with a possible connection to the stimulated release of Fe^{2+}.

B. Electric field perturbation from ferritin is insufficient to directly influence channel proteins

A realistic dynamical model of the magnetic behavior of ferritin is an essential starting point for any analysis of its local inductive effects. Historically, both the reported magnetic properties of ferritin and their interpretations have varied considerably, depending on the biological source and sample preparation. Nevertheless, magnetic characterization of ferritin spans nearly eight decades and can at least inform reasonable bounds for expected behavior.[42] Ferritins occur widely among living organisms, including eukaryotes and some bacteria, and typically consist of a protein shell with an outer diameter of approximately 12 nm and inner diameter of 8 nm surrounding a biomineralized core.[43] The core size varies with iron loading, ranging up to approximately this maximum of 8 nm and has been assumed to be 6 nm in this work to reflect observed size distributions for ferritin used in magnetogenetics research.[40] The size and crystallinity of human ferritin are comparable to those derived from horse spleens, which is often studied. The core consists primarily of ferrihydrite with an approximate stoichiometry $5Fe_2O_3 \cdot 9H_2O$, possibly incorporating trace phosphate impurities.[44,45] Whether attributable to uncompensated antiferromagnetically ordered spins or the existence of multiple phases,[46] several empirical sources contend that ferritin's ferrihydrite core is superparamagnetic at physiological temperatures with a weak magnetic moment of approximately $300 \mu_B$.[21–23] Comparatively recent bimodal magnetic force microscopy measurements of an individual horse spleen ferritin,[47] as well as magnetic characterization of a similar bulk sample,[34] are also consistent with superparamagnetic behavior. A variety of evidence associated with transgenic ferritin, including a measurable influence on T2 relaxation in transfected yeast,[48] magnetic separation in transfected bacteria,[49] and electron micrographs of apparently well-crystalized cores of ferritin expressed by human embryonic kidney cells[40] tend to support the assumption of superparamagnetic properties for transgenic ferritin in vitro or in vivo.

Approximating the moment of ferritin as a $300 \mu_B$ point dipole, the expected field magnitude at its surface is only a few mT and drops to a magnitude comparable to the geomagnetic field within 25 nm. Assuming a voltage-gated ion channel with approximately 10 nm diameter [Fig. 3(a), upper], ferritin directly adjacent to it should produce at most a small field of about 0.4 mT in the center of the channel. While this field magnitude is minute, inductive effects are determined by time-varying flux, and the timescale of fluctuation and precession of the moment plays a role of equal importance in determining this quantity. The effective anisotropy field H_k of ferritin has been estimated from its reported blocking temperature (see supplementary material, Sec. S1). Applying the sLLG model described in Sec. II to ferritin, the resulting time varying field it produces depends on position and fluctuates with frequency contributions spanning several orders of magnitude [Fig. 3(b)]. The precession of the magnetic moment contributes high frequency components to the dB/dt signal, whereas stochastic reversal over the barrier tends to contribute a lower frequency

component. Frequency space representations [Fig. 3(c)] indicate that dB/dt is dominated by precession, in this case peaking in the 100s of GHz. This is a high precession frequency, but a similar order of magnitude has been observed experimentally for iron oxide nanoparticles with moderate anisotropy and low magnetization values.[50] Position (ii) in Figs. 3(b) and 3(c) seems to experience the largest contribution from precession, a consequence of the easy axis serving as the axis of precession and geometric selection of the tangential component.

To provide a basis for comparison, a similar analysis was performed with a 15 nm magnetite MNP situated on the neuronal membrane in the vicinity of a voltage-gated ion channel [Fig. 3(a), lower]. As a result of its rapid precession, ferritin surprisingly manages to generate a dB/dt signal within an order of magnitude compared to this magnetite particle [Fig. 3(d)]. Applying a low pass filter to the signal, the contributions to dB/dt from stochastic reversal of the moment are found to be three orders of magnitude weaker than the one originating from precession [Fig. 3(e)]. These lower frequency components are suppressed in both the case of ferritin and the 15 nm magnetite particle as the applied field increases. Because its exceedingly weak moment and low temperature blocking behavior suggest a strong H_k in the model, a frequency space representation of the dB/dt signal from ferritin reveals that its precession frequency does not depend strongly on applied fields below the scale of 1 T [Fig. 3(f), upper]. By contrast, the considerably lower H_k value for the magnetite particle ensures that its precession frequency increases more than an order of magnitude under an applied field of 1 T [Fig. 3(f), lower]. The fact that the magnitude of the unfiltered dB/dt signal does not increase proportionally with the precession frequency demonstrates a competitive effect between more rapid precession and a magnetic moment more constrained to align with the applied field. Both factors are important in ultimately determining the dB/dt experienced by the voltage-gated ion channel.

Finally, using this model of the dynamic behavior of the moment of ferritin, we considered the voltage induced across the neuronal membrane at the location of the voltage-gated ion channel. The voltage signal is found to be on the scale of 10^{-5} mV, far too small to supply a significant perturbation to the gating charge of the voltage-gated ion channel, which would require 10 s of mV [Fig. 3(f), upper]. The additive dB/dt signal arising from multiple equidistant uncorrelated ferritins increases with the square root of their number (supplementary material, Sec. S4). This effectively rules out the possibility that the combined effect of neighboring ferritins could increase this value by many orders of magnitude. Moreover, even if the magnitude of the perturbative membrane voltage had been far larger, it is not clear whether its frequency in the 100s of GHz would have allowed it to influence the conformation of the voltage-gated ion channel. Despite the appealing logical features of ferritin acting as a source of inductive perturbation on the neuronal membrane for magnetogenetics, our analysis suggests that this hypothesis can probably be ruled out.

C. Induced electric fields on ferritin's mineral core

While ferritin may not act appreciably on the gating charges of nearby channel proteins, local induced electric fields may still be
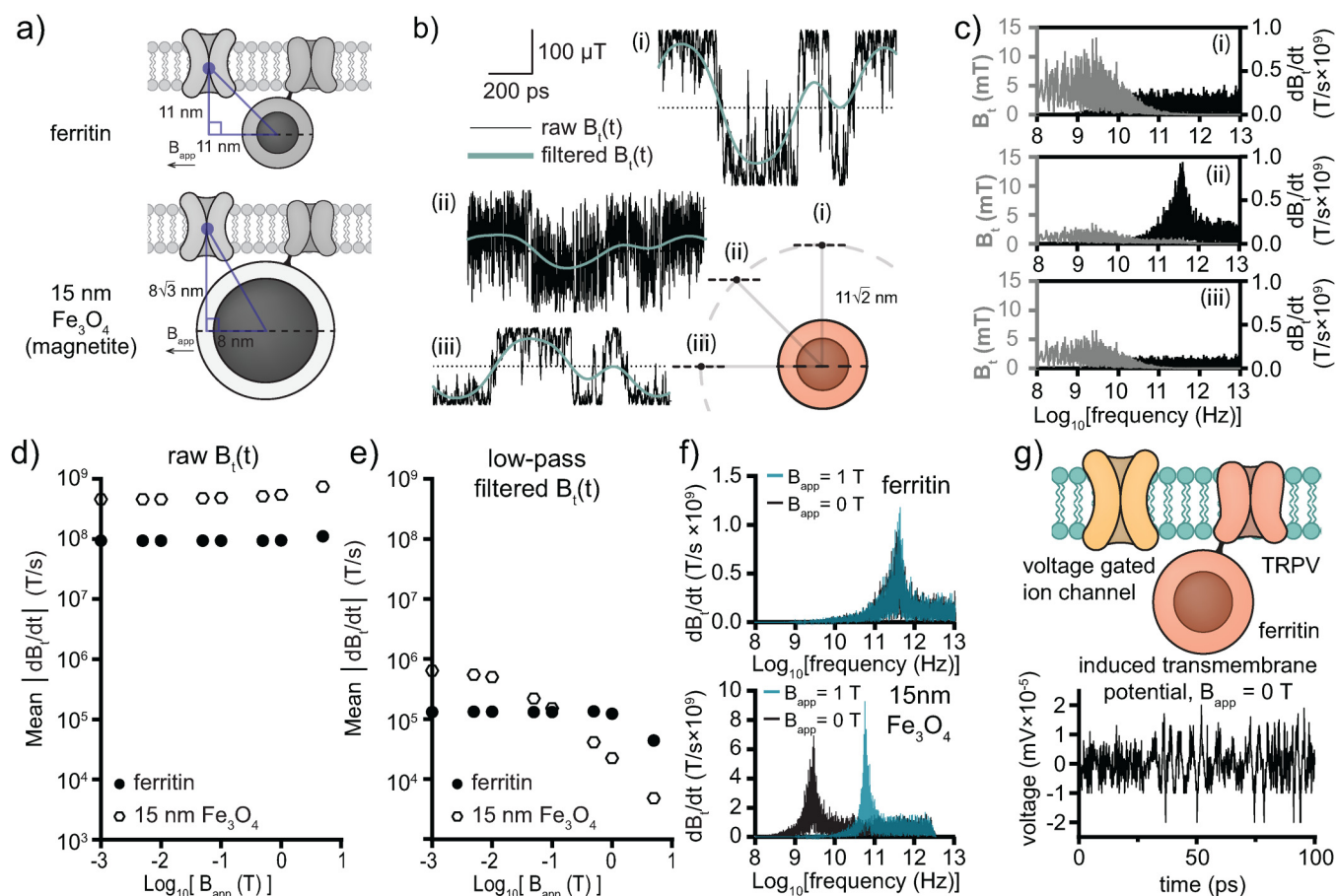
FIG. 3. Testing the hypothesis that ferritin could influence neighboring voltage-gated ion channels with induced electric fields. (a) Simplified geometric assumptions for calculating the component of the field tangential to the membrane are shown explicitly for both a ferritin and a hypothetical 15 nm magnetite particle. (b) 1 ns intervals of the tangential component of the magnetic field vs time at three positions equidistant (15.6 nm) from a simulated ferritin in the absence of an applied field. "Tangential" is defined relative to the direction of the membrane, indicated by the dashed lines. A low pass filter set at 10 GHz reveals the signal resulting from stochastic reversal. The dashed line atop the ferritin indicates the orientation of its easy axis. (c) Frequency domain representations of B (gray) and dB/dt (black) at the three locations (i)–(iii) from (b) are shown using the full duration of the simulation (6×10^6 steps, approx. 233 ns). (d) Time-averaged norm of tangential dB/dt for simulations of 6×10^6 steps each (233 ns for ferritin, 397 ns for magnetite) are shown for a range of applied quasimagnetostatic fields. dB/dt is dominated by the influence of precession. (e) A low pass filter set at 10 GHz for ferritin and 1 GHz for magnetite was applied to the same data represented in panel (d), isolating the applied field dependence of dB/dt originating from stochastic reversal. (f) A frequency space representation of the dB/dt signal from ferritin at no applied field and 1 T shows limited sensitivity to the applied field. A frequency space representation of dB/dt from the 15 nm magnetite particle at 0 and 1 T shows a large influence of the applied field on precession frequency, though not on overall dB/dt magnitude. (g) The transmembrane voltage predicted from electric fields induced by ferritin in the absence of an applied field is shown for 100 ps of dynamical behavior predicted by the sLLG model. The magnitude of this transmembrane voltage, considered at the center of a neighboring voltage-gated ion channel, is too weak to plausibly perturb the gating charge.

hypothesized to play some alternative indirect mechanistic role in magnetogenetic stimulation. Ferritin is primarily an iron storage protein and recent experiments suggest that the release of Fe^{2+} ions from its core and subsequent oxidation of lipids are likely involved in the indirect stimulation of TRPV channel proteins [Fig. 4(a)].[39,40,51] Evidence for the release of Fe^{2+} ions from ferritin in response to radiofrequency magnetic stimuli has included observed bulk colorimetric readouts with ferrozine,[39,41] as well as fluorescence based assays of cytosolic free iron with in vitro cultures.[39] A mechanism for magnetogenetics underpinned by wirelessly stimulated iron ion

release would be more satisfactory if the roles of intrinsic magnetic behavior of ferritin and externally applied magnetic fields in this process could be elucidated. Thus, using our model of ferritin, we additionally considered induced electric fields in the direct vicinity of its mineral core. Biophysical studies indicate the relevance of electrostatic potential gradients within the protein shell of ferritin generated by charged residues of amino acids in facilitating Fe^{2+} ion release,[52] so the net electric field would likely include a combination of the rapid time-varying inductive contribution with a more slowly varying electrostatic contribution.
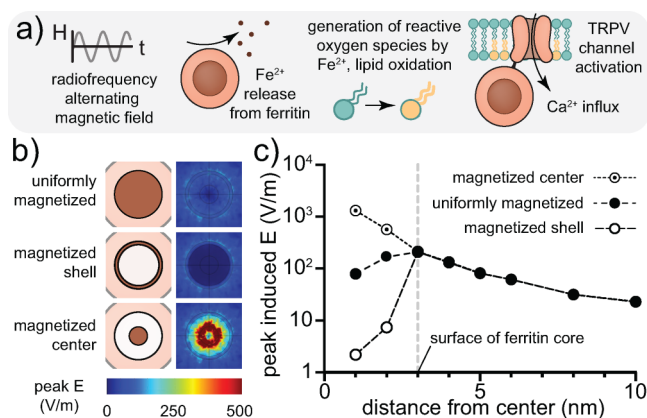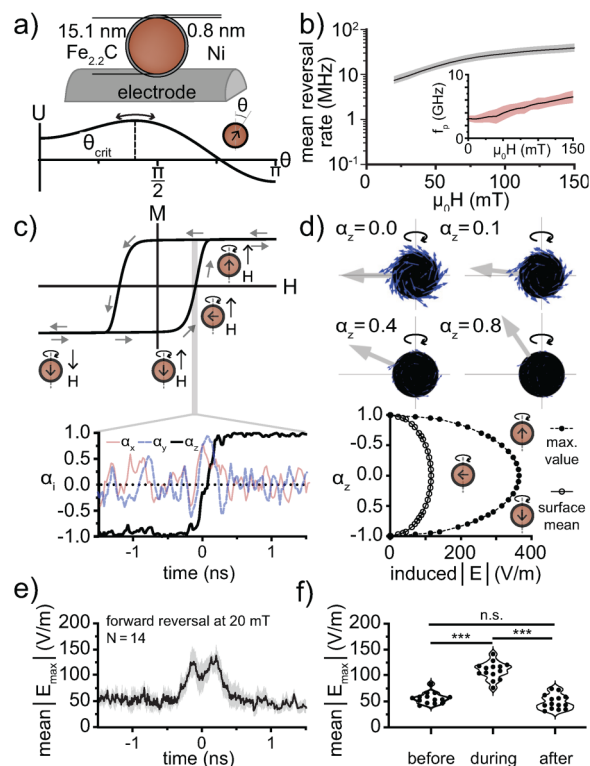
FIG. 4. Considering the possible role of electric fields induced at the surface of ferritin in Fe ion release. (a) Recent studies have suggested that alternating magnetic fields trigger the release of Fe^{2+} from ferritin, leading to reactive oxygen species generation and local lipid oxidation of the membrane that indirectly stimulates the channel protein. (b) Induced electric fields are considered for stable precession at 400 GHz [see Fig. 3(f)], assuming different distributions of magnetization within ferritin, including uniform distribution, uncompensated surface spins, or a more strongly magnetized inclusion. (c) Variation of the magnitude of the peak induced electric field magnitude as a function of distance from the center of ferritin is plotted for the same three cases. At the surface of ferritin and outside, all three converge to similar values.

FIG. 5. Induced electric fields on the surface of catalytic MNPs are elevated during reversal events correlated with hysteresis. (a) Assumed dimensions and composition of the MNPs under study. Magnetic moments were initially set to the critical angle θ_{crit} at which combined energy U is maximized, then proceeding dynamically to either of the two minima. (b) The inverse of the time elapsed until the moment overcomes the barrier to align with the field is defined as the mean reversal rate. Mean reversal rates observed for 40 separate simulations of 10^4 steps (230 ns) are shown for field values at which reversals were observed. The empirically bootstrapped 95% confidence interval for the mean is shaded. The inset shows mean precession frequency f_p extracted from the maxima of FFTs of off-axis components of the magnetization for the full simulations, with shading corresponding to standard deviation ($N = 40$ for each point). (c) An example of an extracted reversal event representing the kind expected during hysteresis heating is shown. (d) Modeling the electric fields induced by stable precession of the magnetic moment at 4.4 GHz indicates considerable dependence on the angle of precession, shown by electric field plots for $\alpha_z = 0.0, 0.1, 0.4, 0.8$. Maximum electric field magnitude and surface averaged electric field magnitude (abscissa) are shown as a function of α_z (ordinate). (e) Maximum electric field magnitude induced at the surface of the catalytic MNP vs time. The mean of all reversal events observed at 20 mT is shown ($N = 14$), with the empirically bootstrapped 95% confidence interval for the mean shaded. (f) Time-averaged maximum induced electric field values were found for the reversal events represented in (e) with averaging windows of 500 ps duration at the times ($-2.0, -1.5$ ns) "before," ($-0.25, 0.25$ ns) "during," and ($1.5, 2.0$ ns) "after." Wilcoxon signed-rank tests assessed the statistical significance of observed differences. ($N = 14$, *** = p-value < 0.0001, n.s. = no significance).

One additional aspect to consider for the induced fields so close to the center of ferritin is the distribution of magnetization within its mineral core. The magnetic properties of ferritin have variously been attributed to uncompensated surface spins or to the existence of internal magnetic phases.[44,46] To account for these possibilities, we considered the case of magnetization confined to the outermost layer (magnetized shell) or to a small central region (magnetized center) in addition to the assumption of uniform magnetization [Fig. 4(b)]. Because precession had been found to dominate the inductive behavior of ferritin [Figs. 3(d)–3(f)], the electric field was simulated for stable precession at the dominant frequency of 400 GHz predicted in Fig. 3(f). It should be noted that although dB/dt peaks around 400 GHz, the frequency of precession in this model of ferritin is somewhat lower, closer to 260 GHz (see supplementary material, Sec. S1).

The magnitude of the expected induced electric fields converges at the surface of the particle for each of the three cases of magnetization distribution that were considered and similarly diminishes with distance [Fig. 4(c)]. On the surface, the maximum magnitude of this induced electric field is predicted to be about 210 V/m. The induced electric fields inside the particles differ markedly for the different magnetization distributions, with the induced field predicted for the magnetized center exceeding 1000 V/m, and the field for the magnetized shell being suppressed to 10s of V/m. If indeed a small region of increased magnetization occurred in ferritin, it would likely not be confined to its geometric center and thus the electric field realized on the surface could be modestly elevated.

Because the electric fields generated by ferritin are predicted to be similar regardless of whether a magnetic field of up to 1 T is applied [Figs. 3(d) and 3(f)], its intrinsically induced electric fields alone cannot be expected to directly liberate Fe ions from the core. Rather, this local effect could become relevant when combined with larger scale ionic currents generated by a time-varying external

field. The capture and release of Fe from ferritin is a chemical equilibrium process, and altered mass transport could influence the kinetics of Fe release, resulting in an effect more subtle than the direct cleavage of chemical bonds or "noise induced transport" within the crystal.[53] In the scenario of Fe ion release limited by mass transport, nanoscale induction by ferritin could serve to increase local ionic diffusivity, whereas ionic transport over longer scales would be driven by macroscopic eddy currents generated by the applied field. Although the influence of magnetic fields on mass transport is often subtle, examples have been noted in which even constant magnetic fields produce observable effects in chemical processes such as electrodeposition or bioelectrocatalytic reactions.[54,55]

A quantitative treatment of the inductive influence of ferritin on local ionic diffusivity goes beyond the scope of the present work, where we have used our model to predict the magnitude and timescale of the locally induced electric field. We emphasize that the predicted electric fields appear to be many orders of magnitude weaker than the electric fields produced by magnetoelectric composite nanoparticles capable of directly triggering chemical reactions, which have been estimated to be as high as 10^7 V/m.[56]

IV. NANOSCALE INDUCTION IN ELECTROCHEMICAL CATALYSIS

A. Unclear mechanism for catalysis enhanced by alternating magnetic fields

Nanoparticles of various compositions and structures have been vigorously studied as heterogenous catalysts to improve the efficiency of a wide range of chemical processes. This includes instances of metallic single domain ferromagnetic nanoparticles, which can be coupled to externally applied AMFs, for instance, to use heat dissipation to control the bulk temperature of a reactor.[57] In a particularly intriguing recent example, an AMF was used to modulate the catalytic enhancement of hydrolysis by iron carbide single domain MNPs coated with a thin layer of nickel that were introduced onto carbon fiber electrodes [Fig. 5(a)]. When an AMF was applied, the presence of these catalytic MNPs was found to reduce the required electrochemical overpotentials by 250 mV at the oxygen evolving electrode and 150 mV at the hydrogen evolving electrode, an enhancement comparable to operating the reaction at approximately 200 °C.[10] Since this effect could not be explained by bulk temperature changes of the reaction solution or other factors, the authors of the study attributed the effect to nanoscale heating of the catalytic MNPs. However, in a subsequent study of chemically similar MNPs monitored by x-ray diffraction while exposed to an AMF, the temperature inside the MNPs matched the bulk temperature within the limits of instrumental uncertainty.[17] Although one interpretation could be that the relevant effects arise from spikes of instantaneous heat flux rather than the establishment of a continuous nanoscale temperature gradient, this serves as yet another striking example in which MNPs have shown clear promise as nanoscale actuators despite an unclear mechanism of action.

Here, we use our computational model of the magnetization dynamics of single domain MNPs to consider whether enhanced nanoscale electric fields are induced by catalytic MNPs during magnetization reversal events modulated by an AMF. One motivation for studying this case is that the reaction in question is electrochemical, providing a more plausible role for nanoscale induced electric fields occurring at the charged interface between the electrode and the solution. Further, it is useful to extend discussion of nanoscale induction to an MNP that is subject to less rapid thermal fluctuation than ferritin and that interacts more robustly with applied fields, since this more closely resembles the majority of cases in which nanoscale effects have been attributed to nanoscale heating. Another reason for selecting the MNPs reported in that particular study of hydrolysis enhancement is that the authors have made sufficient physical characterization data available to select realistic input parameters for modeling.[58]

B. Alternating magnetic fields modulate nanoscale inductive effects in catalytic nanoparticles

Making use of the sLLG model described in Sec. II, spontaneous reversal events were simulated at constant applied field magnitudes. Although AMFs do vary in time, they often do so more slowly than the relevant features of the dynamical behavior of the single domain MNP moments, and it is convenient to consider the influence of the field in its quasistatic limit. Simulations of 10^4 steps spanned a duration of approximately 200 ns, 2% of a full cycle of a field alternating at 100 kHz. The magnitude of the moment of the particle was estimated to be $3.6 \times 10^5 \mu_B$ and the H_k was estimated to be 124 kA/m, values extracted from previously reported supplementary characterization data.[58]

Unlike MNPs consisting of magnetite or other electrically insulating magnetic materials, the effective damping in metallic MNPs is expected to be larger due to interior eddy currents.[59] For the purpose of modeling, two sets of assumptions were separately tested: a "low damping" case of $\kappa = 0.4$ and a "high damping" case of $\kappa = 0.8$, the latter proving more relevant for reproducing empirically observed behavior. (Results from the low damping case are summarized in supplementary material, Sec. S5.) By assuming an initial orientation of the moment at the critical angle θ_{crit} corresponding to the top of the energy barrier separating the easy axes, magnetic moments were allowed to stochastically progress toward either of the energy minima at $\theta = \pi$ or $\theta = 0$ [Fig. 5(a)]. Beginning each simulation at θ_{crit} was intended to sample behavior from each of the minima equally, and the initial transition was excluded from further analysis. The remaining time steps were monitored for further spontaneous transitions over the barrier between the minima.

A minimum of 40 simulations were performed at each applied field value from −150 to 150 mT in steps of 10 mT, with some simulations capturing multiple reversal events. The inverse of the time elapsed since a previous transition reflects the rate of reversal, and the mean of this quantity was determined for a range of applied field amplitudes [Fig. 5(b)]. The overall reversal behavior predicted for the higher damping case is more consistent with the available experimental data for hysteretic heat dissipation as a function of applied field amplitude, which suggests effective trapping of magnetic moments below about 15 mT for these particular MNPs.[58] Precession is again expected to dominate the behavior of the nanoscale induced electric fields, and its frequency is found to be

relatively constant over the 0–50 mT range relevant to the application case, as extracted from fast Fourier transforms of the off-axis components of $\boldsymbol{\alpha}$ [Fig. 5(b), inset].

Because the timescale of reversal events is far shorter than the period of a typical AMF (100s of ps vs a period of 10^7 ps for a 100 kHz AMF), behavior observed at constant applied fields near the minimum magnitude needed to trigger reversals should reflect behavior during reversals that occur during hysteresis. A representative example of the time evolution of magnetic moments during an isolated reversal event is shown in Fig. 5(c), demonstrating a combination of precession and thermal fluctuation.

Considering purely precessional motion of the magnetic moment of the catalytic MNPs at 4.4 GHz reveals a crucial feature of nanoscale induction on the surface: dependence on the angle of precession [Fig. 5(d)]. Inductive effects can be anticipated to depend substantially not only on the frequency, moment, and size of an MNP but also on the instantaneous angle between its moment and the axis of precession. Angles that align the moment with the axis of precession, corresponding to $|\alpha_z| = 1$, suppress induced electric fields, whereas electric field magnitude is maximized when $\alpha_z = 0$ [Fig. 5(d)]. In turn, this suggests that MNPs confining magnetic moments to angles near an easy axis between reversal events should experience a momentary increase in induced electric fields when undergoing precessional motion as they pass through low values of $|\alpha_z|$.

Using our sLLG results for all of the reversal events observed at 20 mT in the $\kappa = 0.8$ case ($N = 14$), the induced electric fields were modeled on their surfaces for a duration of approximately 4.5 ns, centered on the reversal event. Because the timestep for the
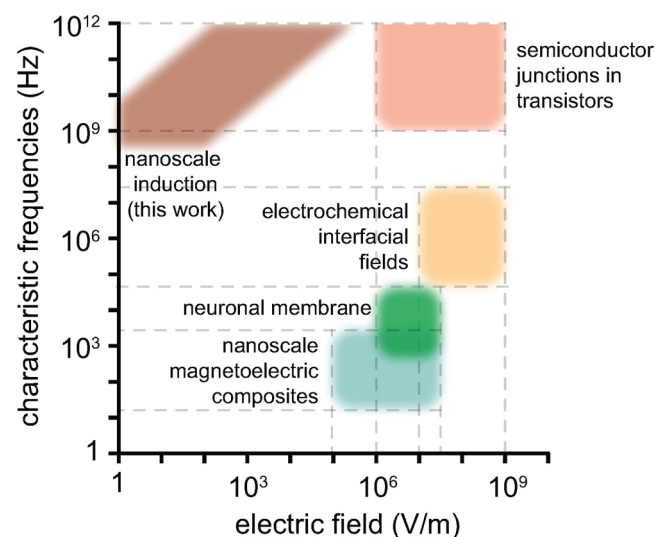
FIG. 6. To provide context, the range of expected electric field magnitudes and characteristic frequencies of variation are shown for a variety of technologically relevant areas. The nanoscale induction bounds represented here are based on the generalized parameter space in Fig. 5(g). Reasoning behind the other phenomena is explained in supplementary material, Sec. S6.

sLLG had been chosen to be relatively large to ensure that long timescales could be simulated for extracting reversal behavior, a 5 timestep averaging filter was applied (approximately 0.36 of a single period of precession) before simulating induced electric fields. Figure 5(e) shows the mean value of the maximum electric field magnitude on the surface of the MNPs as a function of time, with this value clearly elevated immediately before and after the reversal event. To assess whether this peak in electric field magnitude was statistically significant, time-averaged snapshots were computed for 500 ps intervals, 1.75 ns before, during, and 1.75 ns after the reversal events [Fig. 5(f)]. Wilcoxon signed-rank tests confirm that the electric field is statistically significantly higher during the reversal than before or after it. While a difference in the scale of the induced electric field before and after reversal would also be plausible given the different curvature of the local minima [Fig. 5(a)], no significant difference was found.

Taken together, these results suggest that for MNPs capable of effectively thermally trapping moments, the magnitude and extent of induced electric fields are maximized during reversal events. By this reasoning, the generation of these induced electric fields in response to an AMF would be correlated with hysteretic heat dissipation to an extent that would make these effects difficult to distinguish, since effective trapping of moments during the cycle of the AMF is a prerequisite for efficient hysteresis heating via coherent reversal.[60] The peak electric field magnitude was on the order of several hundred V/m, many orders of magnitude weaker than the electric fields existing inside the charged interface that forms on the electrodes and would not be sufficient to trigger electrochemical reactions in isolation. Nevertheless, these fields are far stronger than the initial electric field produced by the electrode that drives the comparatively slow accumulation of charge at its surface when a potential is first applied.[61] Moreover, the direction of the peak electric field induced at the surface of the catalytic MNP is tangential to its surface, with the possibility of introducing electric field components orthogonal to the ones associated with interfacial electrochemical charge accumulation. Thus, either by driving transport within the interface or perturbing the electric field, interaction of these nanoscale induced electric fields with the layers of charges formed at the interface could plausibly influence the process of hydrolysis. The extent of this influence would require modeling of a different sort than the one developed here, and we emphasize that our conclusions are confined to the idea that induced electric fields in the vicinity of MNPs can be correlated with reversal events triggered by AMFs for MNPs with suitable properties for hysteresis heating.

V. CONCLUSION

This work analyzed the external induced electric fields originating from a frequently overlooked aspect of the expected behavior of magnetic nanoparticles emergent at the nanoscale–precession subject to fluctuation of coherent single domains. In particular, we focused on two case studies in which MNPs have shown promise as nanoscale actuators despite unclear or controversial mechanisms of action. In the first case examined, a role was considered for locally induced electric fields generated by the fluctuation and precession of the magnetic moment of ferritin. Despite the surprising

result that ferritin may produce electric fields comparable to a larger magnetite particle, appreciable inductive coupling to voltage-gated channel proteins as a source of perturbation was ruled out as a plausible explanation for magnetogenetic stimulation. Nevertheless, the electric fields induced at the surface of ferritin may still be relevant to the mass transport and release of Fe^{2+} that has been suggested to be mechanistically involved. Applying the same model to a separate case involving catalysis of an electrochemical reaction, we considered the possibility that induced electric fields rather than anomalous nanoscale heating might help to explain the enhancement of hydrolysis by electrodes incorporating MNPs in the presence of an AMF. We found that, for MNPs suited to thermally trap magnetic moments, the induction of nanoscale electric fields is expected to be correlated with reversal events triggered by AMFs.

Because magnetic precession was the dominant influence in determining the character of the local induced field, ferromagnetic resonance may offer the most direct means to experimentally test these ideas. For instance, if nanoscale induced electric fields are indeed responsible for enhancing hydrolysis, it may be worthwhile to repeat that experiment under conditions of ferromagnetic resonance to determine whether the enhancement of hydrolysis could be matched or exceeded. Driving resonant precession of the MNPs could have the further technological advantage of extending the duty cycle of the effect, which is only expected to be intermittent in the presence of an AMF. Similarly, the validity of the model of ferritin could potentially be probed with measurements of ferromagnetic resonance, and the relevance of magnetic precession on Fe ion release or local ionic diffusion could be studied empirically, though the weak magnetic properties of ferritin and very high predicted resonance frequency suggest that such studies could be challenging.

The scale of the fields arising from nanoscale induction was consistently estimated to be comparatively weak, at most on the order of 10^3 V/m for the specific examples considered here. For perspective, Fig. 6 compares the scale of the electric fields involved in a range of technologically relevant phenomena. These values are shown in conjunction with estimates of the relevant timescales at which these fields typically develop and vary, with detailed justification provided in supplementary material, Sec. S6. The characteristic frequencies of nanoscale induction effects tend to be higher than most of the other examples and time average to zero, features that are unsurprising since this induction is dominated by magnetic precession in the GHz frequency range. This implies that the processes most likely to be influenced by inductive effects of MNPs are fast, on the order of ps to ns and involve charged groups, ions, or electrons. For MNPs acting as actuators, the effects attributed to nanoscale heating are often subtle and frequently associated with physical rather than chemical changes, such as liposomal release or influence over the surrounding protein corona. Both lipids and proteins notably bear charged groups, and in such cases, relatively weak yet rapidly varying electric fields produced in the immediate vicinity of MNPs may offer explanatory value.

If nanoscale induced electric fields do indeed play an unappreciated role in localized actuation effects of MNPs, it is worthwhile to consider how single domain MNPs could be engineered to deliberately maximize induced fields at their surfaces. Figure 2(g)

captures the essential parameter space, showing induced electric field normalized to precession frequency in GHz as a function of particle size and magnetization. Since the expected induced field magnitude increases with size, magnetization, and precession frequency, one strategy could be to design MNPs that maximize these quantities. For instance, selecting a metal or metal alloy that has high magnetocrystalline anisotropy would allow larger particles to support a single domain state and would increase the effective H_k, which is predicted by the sLLG equation to raise the frequency of precession. In a biomedical setting, the limited penetration depth of stimuli in the 10s of GHz or higher would likely preclude these MNPs from being driven at resonance. A somewhat counterintuitive alternative strategy could instead be to use relatively large oxide nanoparticles (on the order of 100 nm diameter) with low anisotropy and moderate to low saturation magnetization. This would permit ferromagnetic resonance to be driven at lower frequencies, which might offer the benefit of greater physiological penetration depth of the magnetic stimulus. The intrinsically lower damping expected for oxides due to the lack of eddy currents might also result in sharper resonance and more efficient energy transfer. One challenge that could be anticipated for enlarged nanoparticles is the eventual development of spin wave modes in which the net moment of the MNP is partially canceled.

The number and variety of investigations triggering or enhancing biological and chemical processes in a localized fashion with magnetic nanoparticles has grown substantially in recent years and seems poised to continue. While it may be intuitive to conceptualize the influence of MNPs as a scaled down analog of our macroscopic experience such as nanoscale heating, alternative explanations must be explored when such assumptions are contradicted by both theory and experiment. The local induced electric fields that we have considered here rely on coherent precession and reversal of single domains, making them an emergent phenomenon of nanoscale magnetic materials. Gaining a clearer understanding of the mechanism of nanoscale actuation in these systems, whether through the effect we have examined or through some other influence yet to be identified, is essential for optimizing these systems and envisioning novel techniques for nanoscale actuation.

SUPPLEMENTARY MATERIAL

See the supplementary material for additional methodological details, example code, and figures, as referred to in the main text.

ACKNOWLEDGMENTS

AUTHOR DECLARATIONS
Conflict of Interest

The authors have no conflicts to disclose.

Author Contributions

Michael G. Christiansen: Conceptualization (lead); Data curation (lead); Formal analysis (equal); Investigation (equal); Methodology (equal); Visualization (lead); Writing – original draft (lead); Writing – review & editing (equal). **Nima Mirkhani:** Conceptualization (supporting); Data curation (equal); Investigation (equal); Methodology (equal); Visualization (equal); Writing – review & editing (equal). **William Hornslien:** Investigation (equal); Visualization (equal); Writing – review & editing (supporting). **Simone Schuerle:** Conceptualization (supporting); Funding acquisition (equal); Supervision (lead); Writing – review & editing (equal).

DATA AVAILABILITY

The data that support the findings of this study are available from the corresponding author upon reasonable request.

REFERENCES

[1]Y. Zhang, Y. Wang, Q. Zhou, X. Chen, W. Jiao, G. Li, M. Peng, X. Liu, Y. He, and H. Fan, "Precise regulation of enzyme–nanozyme cascade reaction kinetics by magnetic actuation toward efficient tumor therapy," ACS Appl. Mater. Interfaces 44, 52395–52405 (2021).

[2]H. Zhang, J. Li, Y. Chen, J. Wu, K. Wang, L. Chen, Y. Wang, X. Jiang, Y. Liu, Y. Wu et al., "Magneto-electrically enhanced intracellular catalysis of FePt-FeC heterostructures for chemodynamic therapy," Adv. Mater. 33, 2100472 (2021).

[3]E. Amstad, J. Kohlbrecher, E. Müller, T. Schweizer, M. Textor, and E. Reimhult, "Triggered release from liposomes through magnetic actuation of iron oxide nanoparticle containing membranes," Nano Lett. 11, 1664–1670 (2011).

[4]S. Schuerle, J. S. Dudani, M. G. Christiansen, P. Anikeeva, and S. N. Bhatia, "Magnetically actuated protease sensors for in vivo tumor profiling," Nano Lett. 16, 6303–6310 (2016).

[5]S. Rao, R. Chen, A. A. LaRocca, M. G. Christiansen, A. W. Senko, C. H. Shi, P.-H. Chiang, G. Varnavides, J. Xue, Y. Zhou et al., "Remotely controlled chemo-magnetic modulation of targeted neural circuits," Nat. Nanotechnol. 14, 967–973 (2019).

[6]T. Zhang, G. Li, Y. Miao, J. Lu, N. Gong, Y. Zhang, Y. Sun, Y. He, M. Peng, X. Liu et al., "Magnetothermal regulation of in vivo protein corona formation on magnetic nanoparticles for improved cancer nanotherapy," Biomaterials 276, 121021 (2021).

[7]S. A. Stanley, J. E. Gagner, S. Damanpour, M. Yoshida, J. S. Dordick, and J. M. Friedman, "Radio-wave heating of iron oxide nanoparticles can regulate plasma glucose in mice," Science 336, 604–608 (2012).

[8]M. A. Wheeler, C. J. Smith, M. Ottolini, B. S. Barker, A. M. Purohit, R. M. Grippo, R. P. Gaykema, A. J. Spano, M. P. Beenhakker, S. Kucenas et al., "Genetically targeted magnetic control of the nervous system," Nat. Neurosci. 19, 756–761 (2016).

[9]J. G. Ovejero, I. Armenia, D. Serantes, S. Veintemillas-Verdaguer, N. Zeballos, F. López-Gallego, C. Grüttner, J. M. de la Fuente, M. d. Puerto Morales, and V. Grazu, "Selective magnetic nanoheating: Combining iron oxide nanoparticles for multi-hot-spot induction and sequential regulation," Nano Lett. 21, 7213–7220 (2021).

[10]C. Niether, S. Faure, A. Bordet, J. Deseure, M. Chatenet, J. Carrey, B. Chaudret, and A. Rouet, "Improved water electrolysis using magnetic heating of FeC-Ni core-shell nanoparticles," Nat. Energy 3, 476–483 (2018).

[11]P. Keblinski, D. G. Cahill, A. Bodapati, C. R. Sullivan, and T. A. Taton, "Limits of localized heating by electromagnetically excited nanoparticles," J. Appl. Phys. 100, 054305 (2006).

[12]M. Honda, Y. Saito, N. I. Smith, K. Fujita, and S. Kawata, "Nanoscale heating of laser irradiated single gold nanoparticles in liquid," Opt. Express 19, 12375–12383 (2011).

[13]A. Espinosa, G. R. Castro, J. Reguera, C. Castellano, J. Castillo, J. Camarero, C. Wilhelm, M. A. García, and Á. Muñoz-Noval, "Photoactivated nanoscale temperature gradient detection using x-ray absorption spectroscopy as a direct nano-thermometry method," Nano Lett. 21, 769–777 (2020).

[14]A. Riedinger, P. Guardia, A. Curcio, M. A. Garcia, R. Cingolani, L. Manna, and T. Pellegrino, "Subnanometer local temperature probing and remotely controlled drug release based on azo-functionalized iron oxide nanoparticles," Nano Lett. 13, 2399–2406 (2013).

[15]H. Huang, S. Delikanli, H. Zeng, D. M. Ferkey, and A. Pralle, "Remote control of ion channels and neurons through magnetic-field heating of nanoparticles," Nat. Nanotechnol. 5, 602–606 (2010).

[16]H. C. Davis, S. Kang, J.-H. Lee, T.-H. Shin, H. Putterman, J. Cheon, and M. G. Shapiro, "Nanoscale heat transfer from magnetic nanoparticles and ferritin in an alternating magnetic field," Biophys. J. 118, 1502–1510 (2020).

[17]S. Faure, N. Mille, S. S. Kale, J. M. Asensio, J. Marbaix, P. Farger, D. Stoian, W. van Beek, P.-F. Fazzini, K. Soulantica et al., "Internal temperature measurements by x-ray diffraction on magnetic nanoparticles heated by a high-frequency magnetic field," J. Phys. Chem. C 124, 22259–22265 (2020).

[18]M. Barbic, "Possible magneto-mechanical and magneto-thermal mechanisms of ion channel activation in magnetogenetics," eLife 8, e45807 (2019).

[19]W. F. Brown Jr, "Thermal fluctuations of a single-domain particle," Phys. Rev. 130, 1677 (1963).

[20]M. Meister, "Physical limits to magnetogenetics," eLife 5, e17210 (2016).

[21]S. Kilcoyne and R. Cywinski, "Ferritin: A model superparamagnet," J. Magn. Magn. Mater. 140, 1466–1467 (1995).

[22]S. A. Makhlouf, F. Parker, and A. Berkowitz, "Magnetic hysteresis anomalies in ferritin," Phys. Rev. B 55, R14717 (1997).

[23]R. A. Brooks, J. Vymazal, R. B. Goldfarb, J. W. Bulte, and P. Aisen, "Relaxometry and magnetometry of ferritin," Magn. Reson. Med. 40, 227–235 (1998).

[24]P. Ramachandran and G. Varoquaux, "Mayavi: 3D visualization of scientific data," Comput. Sci. Eng. 13, 40–51 (2011).

[25]M. Lakshmanan, "The fascinating world of the Landau–Lifshitz–Gilbert equation: An overview," Philos. Trans. R. Soc., A 369, 1280–1300 (2011).

[26]N. Usov, "Low frequency hysteresis loops of superparamagnetic nanoparticles with uniaxial anisotropy," J. Appl. Phys. 107, 123909 (2010).

[27]D. B. Reeves and J. B. Weaver, "Nonlinear simulations to optimize magnetic nanoparticle hyperthermia," Appl. Phys. Lett. 104, 102403 (2014).

[28]W. Wernsdorfer, E. B. Orozco, K. Hasselbach, A. Benoit, B. Barbara, N. Demoncy, A. Loiseau, H. Pascard, and D. Mailly, "Experimental evidence of the Néel-Brown model of magnetization reversal," Phys. Rev. Lett. 78, 1791 (1997).

[29]L. Néel, "Théorie du traînage magnétique des ferromagnétiques en grains fins avec applications aux terres cuites," Ann. Géophys. 5, 99–136 (1949).

[30]P. Fannin and S. Charles, "On the calculation of the Neel relaxation time in uniaxial single-domain ferromagnetic particles," J. Phys. D: Appl. Phys. 27, 185 (1994).

[31]S. M. Sternson and B. L. Roth, "Chemogenetic tools to interrogate brain functions," Annu. Rev. Neurosci. 37, 387–407 (2014).

[32]N. A. Repina, A. Rosenbloom, A. Mukherjee, D. V. Schaffer, and R. S. Kane, "At light speed: Advances in optogenetic systems for regulating cell signaling and behavior," Annu. Rev. Chem. Biomol. Eng. 8, 13–39 (2017).

[33]F.-X. Xu, L. Zhou, X.-T. Wang, F. Jia, K.-Y. Ma, N. Wang, L. Lin, F.-Q. Xu, and Y. Shen, "Magneto is ineffective in controlling electrical properties of cerebellar purkinje cells," Nat. Neurosci. 23, 1041–1043 (2020).

[34]D. Liße, C. Monzel, C. Vicario, J. Manzi, I. Maurin, M. Coppey, J. Piehler, and M. Dahan, "Engineered ferritin for magnetogenetic manipulation of proteins and organelles inside living cells," Adv. Mater. 29, 1700189 (2017).

[35]M. C. Romero, M. Davare, M. Armendariz, and P. Janssen, "Neural effects of transcranial magnetic stimulation at the single-cell level," Nat. Commun. 10, 1–11 (2019).

[36]T. Wagner, A. Valero-Cabre, and A. Pascual-Leone, "Noninvasive human brain stimulation," Annu. Rev. Biomed. Eng. 9, 527–565 (2007).

[37]E. U. Saritas, P. W. Goodwill, and S. M. Conolly, "Effects of pulse duration on magnetostimulation thresholds," Med. Phys. **42**, 3005–3012 (2015).

[38]M. A. Wheeler, C. D. Deppmann, M. K. Patel, and A. D. Güler, "Reply to: Magneto is ineffective in controlling electrical properties of cerebellar purkinje cells, assessing the utility of Magneto to control neuronal excitability in the somatosensory cortex and revaluation of magnetic properties of Magneto," Nat. Neurosci. **23**, 1051–1054 (2020).

[39]M. Hernández-Morales, T. Shang, J. Chen, V. Han, and C. Liu, "Lipid oxidation induced by RF waves and mediated by ferritin iron causes activation of ferritin-tagged ion channels," Cell Rep. **30**, 3250–3260 (2020).

[40]M. I. Brier, J. W. Mundell, X. Yu, L. Su, A. Holmann, J. Squeri, B. Zhang, S. A. Stanley, J. M. Friedman, and J. S. Dordick, "Uncovering a possible role of reactive oxygen species in magnetogenetics," Sci. Rep. **10**, 1–13 (2020).

[41]O. Céspedes and S. Ueno, "Effects of radio frequency magnetic fields on iron release from cage proteins," Bioelectromagnetics **30**, 336–342 (2009).

[42]L. Michaelis, C. D. Coryell, and S. Granick, "Ferritin III. The magnetic properties of ferritin and some other colloidal ferric compounds," J. Biol. Chem. **148**, 463–480 (1943).

[43]D. He and J. Marles-Wright, "Ferritin family proteins and their use in bionanotechnology," New Biotechnol. **32**, 651–657 (2015).

[44]N. D. Chasteen and P. M. Harrison, "Mineralization in ferritin: An efficient means of iron storage," J. Struct. Biol. **126**, 182–194 (1999).

[45]G. Jutz, P. van Rijn, B. Santos Miranda, and A. Böker, "Ferritin: A versatile building block for bionanotechnology," Chem. Rev. **115**, 1653–1701 (2015).

[46]J. Cowley, D. E. Janney, R. Gerkin, and P. R. Buseck, "The structure of ferritin cores determined by electron nanodiffraction," J. Struct. Biol. **131**, 210–216 (2000).

[47]L. Stühn, J. Auernhammer, and C. Dietz, "pH-depended protein shell dis-and reassembly of ferritin nanoparticles revealed by atomic force microscopy," Sci. Rep. **9**, 1–9 (2019).

[48]Y. Matsumoto, R. Chen, P. Anikeeva, and A. Jasanoff, "Engineering intracellular biomineralization and biosensing by a magnetic protein," Nat. Commun. **6**, 1–10 (2015).

[49]X. Liu, P. A. Lopez, T. W. Giessen, M. Giles, J. C. Way, and P. A. Silver, "Engineering genetically-encoded mineralization and magnetism via directed evolution," Sci. Rep. **6**, 1–10 (2016).

[50]E. Gorbachev, M. Soshnikov, M. Wu, L. Alyabyeva, D. Myakishev, E. Kozlyakova, V. Lebedev, E. Anokhin, B. Gorshunov, O. Brylev et al., "Tuning the particle size, natural ferromagnetic resonance frequency and magnetic properties of ε-Fe_2O_3 nanoparticles prepared by a rapid sol–gel method," J. Mater. Chem. C **9**, 6173–6179 (2021).

[51]M. Hernández-Morales, V. Han, R. H. Kramer, and C. Liu, "Evaluating methods and protocols of ferritin-based magnetogenetics," iScience **24**, 103094 (2021).

[52]D. Sala, S. Ciambellotti, A. Giachetti, P. Turano, and A. Rosato, "Investigation of the iron (II) release mechanism of human H-ferritin as a function of pH," J. Chem. Inf. Model. **57**, 2112–2118 (2017).

[53]A. Mielke, "Noise induced transport," Ann. Phys. **507**, 476–500 (1995).

[54]A. Wang, Q. Deng, L. Deng, X. Guan, and J. Luo, "Eliminating tip dendrite growth by Lorentz force for stable lithium metal anodes," Adv. Funct. Mater. **29**, 1902630 (2019).

[55]E. Katz, O. Lioubashevski, and I. Willner, "Magnetic field effects on bioelectrocatalytic reactions of surface-confined enzyme systems: Enhanced performance of biofuel cells," J. Am. Chem. Soc. **127**, 3979–3988 (2005).

[56]F. Mushtaq, X. Chen, H. Torlakcik, C. Steuer, M. Hoop, E. C. Siringil, X. Marti, G. Limburg, P. Stipp, B. J. Nelson et al., "Magnetoelectrically driven catalytic degradation of organics," Adv. Mater. **31**, 1901378 (2019).

[57]P. M. Mortensen, J. S. Engbæk, S. B. Vendelbo, M. F. Hansen, and M. Østberg, "Direct hysteresis heating of catalytically active Ni–Co nanoparticles as steam reforming catalyst," Ind. Eng. Chem. Res. **56**, 14006–14013 (2017).

[58]A. Bordet, L.-M. Lacroix, P.-F. Fazzini, J. Carrey, K. Soulantica, and B. Chaudret, "Magnetically induced continuous CO_2 hydrogenation using composite iron carbide nanoparticles of exceptionally high heating power," Angew. Chem. Int. Ed. **55**, 15894–15898 (2016).

[59]S. Denisov, T. Lyutyy, B. Pedchenko, and H. Babych, "Eddy current effects in the magnetization dynamics of ferromagnetic metal nanoparticles," J. Appl. Phys. **116**, 043911 (2014).

[60]J. Carrey, B. Mehdaoui, and M. Respaud, "Simple models for dynamic hysteresis loop calculations of magnetic single-domain nanoparticles: Application to magnetic hyperthermia optimization," J. Appl. Phys. **109**, 083921 (2011).

[61]M. Z. Bazant, K. Thornton, and A. Ajdari, "Diffuse-charge dynamics in electrochemical systems," Phys. Rev. E **70**, 021506 (2004).